Accepted for publication in ApJ

Emission Line Variability of the Accreting Young Brown Dwarf 2MASSW J1207334-393254: From Hours to Years

Beate Stelzer

INAF – Osservatorio Astronomico di Palermo, Piazza del Parlamento 1, 90134 Palermo, Italy

stelzer@astropa.unipa.it

and

Alexander Scholz

SUPA, School of Physics and Astronomy, University of St.Andrews, North Haugh, St. Andrews, Fife KY 16 9SS, United Kingdom

and

Ray Jayawardhana

Department of Astronomy & Astrophysics, University of Toronto, 50 St. George Street, Toronto, ON M5S 3H4, Canada

ABSTRACT

We have obtained a series of high-resolution optical spectra for 2MASSW J1207334-393254 (2M 1207). Two consecutive observing nights at the ESO Very Large Telescope with the UVES spectrograph yielded a timeseries with a resolution of $\sim$ 12 min. Additional high-resolution optical spectra were obtained months apart at the Magellan Clay telescope using the MIKE instrument. Combined with previously published results, these data allow us to investigate changes in the emission line spectrum of 2M 1207 on timescales of hours to years. Most of the emission line profiles of 2M 1207 are broad, in particular that of Hα, indicating that the dominant fraction of the emission must be attributed to disk accretion rather than to magnetic activity. From the Hα 10 % width we deduce a relatively stable accretion rate between $10^{-10.1...-9.8}\,M_{\odot}$/yr for two nights of consecutive observations. Therefore, either the accretion stream is nearly homogeneous over (sub-)stellar longitude or the system is seen face-on. Small but significant variations are evident throughout our near-continuous observation, and they reach a maximum after ~ 8 h, roughly the timescale on which maximum variability is expected across the rotation cycle. Together with past measurements, we confirm that the accretion rate of 2M 1207 varies by more than one order of magnitude on timescales of months to years. Such variable mass accretion yields a plausible explanation for the observed spread in the $\dot{M} - M$ diagram. The magnetic field required to drive the funnel flow is on the order of a few hundred G. Despite the obvious presence of a magnetic field, no radio nor X-ray emission has been reported for 2M 1207. Possibly strong accretion suppresses magnetic activity in brown dwarfs, similar to the findings for higher mass T Tauri stars.

Subject headings: Accretion, Accretion Disks – Stars: Low-Mass, Brown Dwarfs – Stars: Circumstellar Matter – Line: Formation, Profiles – Stars: Planetary Systems

1. Introduction

In recent years, there is increasing evidence that young brown dwarfs evolve similarly to their higher-mass counterparts, the T Tauri stars (TTS). In particular, their formation process includes a phase of mass accretion from a circumstellar disk, whose presence is probed by infrared emission in excess of the photosphere (e.g., Natta et al. 2002; Jayawardhana et al. 2003a; Luhman et al. 2005; Allers et al. 2006). Spectroscopic features, such as the strength and shape of Hα emission, directly trace the accreting material. In the stellar regime, 'weak TTS' have no optically thick circumstellar matter, and their Hα emission is purely chromospheric. In 'classical TTS', the line emission is dominated by contributions from accretion. Next to displaying much stronger lines, their line profiles are broader due to the high velocities in the accreting gas and Stark broadening (Muzerolle et al. 2001). Winds may play a role as well, and are recognized by blueshifted absorption components and forbidden emission lines (Mundt 1984; Edwards et al. 1987; Hamann 1994; Hartigan et al. 1995). Analogous observations have been made for brown dwarfs, where classical TTS-like Hα emission persists down to the deuterium burning limit (Mohanty et al. 2005). Forbidden emission lines, tracing outflows have been reported from a small number of brown dwarfs (e.g., Fernández & Comerón 2001; Barrado y Navascués et al. 2004).

Brown dwarfs are intrinsically faint objects, therefore a detailed study of magnetic activity and accretion in young brown dwarfs is restricted to the most nearby ones. A particularly well-suited playground is the TW Hya association (TWA), with four confirmed brown dwarfs at an age of ~ 8 Myr and a distance of ~ 50 pc. 2M 1207 is the best-studied among the brown dwarfs in the TWA. Its youth was confirmed by low gravity and Lithium absorption, and its TWA membership by radial velocity and proper motion studies (Gizis 2002; Mohanty et al. 2003; Scholz et al. 2005b). Mamajek (2005) has revised the previous distance estimate of 2M 1207 using the moving cluster method, resulting in 53 ± 6 pc. 2M 1207 is the oldest brown dwarf known to actively accrete from a disk, thus representing a benchmark in constraining the disk lifetimes in the substellar regime. The object has recently aroused strong interest because of the discovery of a planetary mass companion (Chauvin et al. 2004, 2005). This companion is at a separation of 40 AU and not expected to influence the magnetic and accretion activity of the brown dwarf.

Stellar astronomers are intrigued by 2M 1207 being the closest known brown dwarf with a disk. No substantial L' excess was detected by Jayawardhana et al. (2003a), but mid-IR photometry established the presence of circumstellar material (Sterzik et al. 2004). This is also corroborated by *Spitzer* photometry, where 2M 1207 is detected in all IRAC bands and at $24\,\mu$m above photospheric levels (Riaz et al. 2006). The spectral energy distribution of 2M 1207 shows evidence for dust evolution, similar to the higher-mass disk-bearing TTS in the TWA. 2M 1207 is therefore a lower-mass analog of the classical TTS.

Strong Hα emission has been reported right with the identification of 2M 1207 as a TWA candidate (Gizis 2002). Subsequent high-resolution spectra have shown that the Hα profile is broadened and asymmetric, thus displaying characteristic signatures of accretion (Mohanty et al. 2003). The Hα equivalent width measured by Mohanty et al. (2003) was only about one-tenth of the earlier value obtained by Gizis (2002), and this variability was interpreted as a sign for variable mass accretion rate. In a subsequent study of emission line variability, aiming at constraining these variations, 2M 1207 presented dramatic changes in the shape and intensity of its Hα line in data obtained two months apart (Scholz et al. 2005a). The observed profile variability was consistent with a scenario of asymmetric accretion with a direct view into the (magnetic) funnel flow (Scholz & Jayawardhana 2006). In this picture, variability is also expected on the time scale of the rotation period (~ 1 d), as the hot accretion spots are corotating with the star. Existing data have remained inconclusive in this respect due to poor sampling. Therefore, we have collected new high spectral resolution data with the aim to monitor the Hα variability on shorter time scales.

Here we present the results obtained during two consecutive nights of observation, and from five additional spectra taken weeks to months apart. The observations are described in Sect. 2. In Sect. 3 we present a detailed analysis of the characteristics of the Hα emission and other prominent emission lines in the optical spectrum of 2M 1207. The results are discussed in Sect. 4, where the spectral variability is examined on various timescales from hours to years. Estimates for the accretion rate and the magnetic field strength of 2M 1207 are presented, and put in context with other (sub)stellar objects. Finally, we compare the accretion and activity characteristics of all known brown dwarfs in TWA. Concluding remarks are found in Sect. 5.

2. Observations

2M 1207 was observed with the *Ultraviolet and Visual Echelle Spectrograph* (UVES) at the ESO VLT 2 during two nights May 8-9, 2006 in the dichroic mode that covers the full spectral range of UVES by simultaneous use of both the blue and the red arm. We used the standard setting DICHR #2 centered at 437 nm for the blue arm and at 760 nm for the red arm. This setup yields simultaneous spectral coverage from $3730 - 4990$ Å on the blue chip and from $5650 - 9460$ Å on the red mosaic. A slit width of $0.8''$ was chosen resulting in a resolving power $R \approx 50000$. The CCDs were rebinned to 2×2 pixels.

The integration time was 600 s. During the two observing nights, we obtained a total of 59 exposures of 2M 1207 at blue and red wavelengths. Except for some constraints due to calibrations and weather the frames were taken consecutively, such that the time resolution for the investigation of spectral changes is ~ 12 min over a large part of the observations.

The data were processed with the UVES pipeline implemented in the MIDAS environment (Ballester et al. 2000). Reduction steps included bias subtraction, flatfield correction, and wavelength calibration. The final one-dimensional spectra have been corrected for contaminating sky light and cosmic rays have been removed. Each spectrum was corrected for the radial velocity of 2M 1207 (11.2 km/s; Mohanty et al. 2003) and for the barycenter motion of the Earth.

We extracted a spectrum from each of the individual science frames. In addition, to increase the S/N for the detection and measurements of weak spectral features, we built averages of each four consecutive frames. Thus, the effective exposure times of these merged spectra are 40 min. Three individual frames with poor S/N were not considered in the merging process, such that we obtain 14 average spectra from the two nights. The spectra were rebinned to $R = 50000$ around individual emission lines before the scientific analysis was carried out.

In February and April 2006, we obtained five additional exposures of 2M 1207 using the Magellan Inamori Kyocera Echelle (MIKE) spectrograph at the Magellan Clay telescope on Las Campanas, Chile. These data were reduced using standard routines within IRAF, including bias subtraction, flatfielding, wavelength and relative flux calibration, and removal of cosmic rays. For more details of the reduction procedure, see Scholz & Jayawardhana (2006). Exposure times for the MIKE spectra were typically 10 min, and the nominal resolution is $R \approx 25000$.

3. Emission line spectrum

3.1. Hα emission

The main aim of this study is to examine the variability of the Hα emission of 2M 1207 with good time resolution and on time-scales of ~ 1 d, corresponding to its suspected rotation period. An estimate for the period is given by Scholz et al. (2005a). In brief, the rotational velocity of 2M 1207 is $v \sin i = 13 \pm 2$ km/s (Mohanty et al. 2003). Together with a radius of $0.27\,R_{\odot}$ extracted from evolutionary models (Chabrier et al. 2000), the period is expected to be $P/\sin i \approx 25.2$ h. Assuming a random position for the inclination, the most probable value for $\sin i$ is 0.81, and for this value the rotation period is 20.4 h. Magnetospheric accretion models (Hartmann et al. 1994) have shown that the presence of a red absorption feature in the Balmer lines (frequently seen in 2M 1207; see below) indicates high inclination. For $i \geq 60°$ the expected period is ≥ 22 h.

The Hα emission of 2M 1207 is thought to be dominated by accretion: the broad wings with velocities of up to ± 200 km/s can not be explained by magnetic activity, the rotational velocity is comparatively small and can not be responsible for the broad wings, and signatures for winds are very weak (Mohanty et al. 2005; Whelan et al. 2007).

The most widely used indicator for identifying accreting stars is the equivalent width $W_{\rm EQ}$ of the Hα line, where weak emission is due to chromospheric magnetic activity and strong emission, above a certain threshold of $W_{\rm EQ}$, is attributed to accretion. However, its dependence on the continuum level precludes $W_{\rm EQ}$ as a universal measure. To take account of the declining continuum for later spectral types, the threshold for $W_{\rm EQ}$ that separates accretors from non-accretors among TTS is usually adapted in discrete steps from ~ 5 Å for spectral types earlier than M0 to something like 20 Å for late M-type stars (Martín 1998). Furthermore, equivalent width measurements of faint continuum sources such as brown dwarfs are intrinsically associated with considerable uncertainties. This is due to the low S/N and the presence of overlapping absorption features that form a 'pseudo-continuum' which depends on the spectral resolution. To avoid these problems, following a suggestion by White & Basri (2003), the full width at 10 % of the peak height ($W_{10\,\%}$) of Hα has been established as more reliable accretion indicator: Objects with $W_{10\,\%} > 200$ Å can be considered accretors (Jayawardhana et al. 2003b).

3.1.1. Profiles and line widths

We use $W_{10\,\%}$ as the primary accretion indicator, but examine also other parameters that characterize the line intensity and shape. Fig. 1 shows the time-series of these parameters obtained during our run with UVES on May 8-9, 2006. The 10 % width is clearly above the accretion threshold throughout our observation ($W_{10\,\%} \approx 280...320\,\mathrm{km/s}$); on average it is higher during the second night, in the course of which it slightly declines. The equivalent width has ups and downs during the first night, and has its maximum at the beginning of the second night, after which it declines dramatically and in a continuous way until the end of the observation. The errors in W_{EQ} are dominated by the (faint) continuum level. We estimated the uncertainty of the continuum flux by varying the sky extraction area, and found that it is of the order of 15 %. Then we computed error bars for W_{EQ} assuming for the continuum flux $0.85 \cdot I_{\mathrm{cont}}$ and $1.15 \cdot I_{\mathrm{cont}}$, respectively. Fig. 1 shows that when taking into account these uncertainties, the observed variations of W_{EQ} remain significant.

The Hα emission is double-peaked throughout all our observations from February to May 2006. Fig. 2 displays the time-series of all 14 normalized average line profiles $\bar{I}_{\mathrm{n}}(\lambda)$ from the UVES run (May 2006), and Fig. 3 shows the 5 normalized profiles obtained with MIKE (February and April 2006). For clarity, in Figs. 2 and 3 the individual spectra have been shifted with respect to each other in the vertical direction.

Scholz et al. (2005a) have shown that the double-peaked Hα profile of 2M 1207 can be interpreted as a broad emission line onto which a red-shifted absorption component is superposed. For the minimum of the absorption feature we measure a position that varies in the range $\Delta v_{\mathrm{min}} \approx -10... + 70\,\mathrm{km/s}$ with respect to the expected wavelength ($\Delta v_{\mathrm{min}} \approx +30... + 70\,\mathrm{km/s}$ in February 2006, $\Delta v_{\mathrm{min}} \approx +10\,\mathrm{km/s}$ in April 2006, and $\Delta v_{\mathrm{min}} \approx -10... + 40\,\mathrm{km/s}$ in May 2006). From Fig. 1 it appears that twice during the extensive monitoring in May 2006 v_{min} undergoes a discrete jump from high redshift towards the expected line center. These times correspond to line profiles in which the absorption trough is wide and asymmetric, such that the position of the minimum can not be determined precisely (Fig. 2). As a measure for the asymmetry of the emission component, Fig. 1 shows the difference between the 10 % width on the blue (left) and on the red (right) side of $\Delta v = 0$. In the course of the UVES observations, $W_{10\,\%}(l - r)$ varied from $-40... + 40\,\mathrm{km/s}$. In particular, during the second night the line moved systematically from the blue to the red. This is in contrast to the absorption feature shown above to be redwards of $\Delta v = 0$ throughout the observation (cf. also Fig. 2).

We examined the shape of the Hα line and its change in time by modeling each of the 14 average profiles with two quasi-Gaussians, one with positive normalization representing the emission component and one with negative normalization for the absorption component.

Each of these has three free parameters (position, width, and normalization). The equivalent widths of the emission $W_{\rm EQ;em}$ and the absorption $W_{\rm EQ;abs}$ component derived from the fits turn out to be strongly correlated (Fig. 4). Since $W_{\rm EQ;em}$ is by definition 'normalized' to the continuum this relation is not trivial. In Fig. 4 we also plot the *observed* flux, i.e. the difference between the flux in the emission profile and the absorption profile, versus the 10 % width.

The Hα 10 % width of 2M 1207 has been measured at eight epochs so far (see Table 1). In most of the high-resolution spectra collected so far 2M 1207 showed $W_{10\,\%}$ clearly above the accretion threshold, although in some occasions there were only marginal signs of accretion ($W_{10\,\%} \sim 200\,$km/s).

3.1.2. Quantifying variability

To quantify the Hα variability as a function of wavelength we examined the normalized variance profile

$$\sigma^2_{\rm n}(\lambda) = \sigma^2(\lambda)/\bar{I}_{\rm n}(\lambda), \tag{1}$$

where the variance profile $\sigma^2(\lambda) = \frac{1}{N-1}\sum_{i=1}^{N}\left[I_{\rm n,i}(\lambda) - \bar{I}_{\rm n}(\lambda)\right]^2$ measures flux variations across the line profile (Johns & Basri 1995). In the bottom panels of Fig.2 we plot $\sqrt{\sigma^2_{\rm n}}$ for three distinct parts of the observation in May 2006. From left to right, are shown the variances obtained from all 19 spectra from the first night, the first 20 and the last 20 spectra of the second night, respectively. This way, the individual $\sqrt{\sigma^2_{\rm n}}$ give information about the variations as a function of wavelength on short time-scales (within the $\sim 4\,$h covered by 19 respectively 20 consecutive frames), and a comparison of the different $\sqrt{\sigma^2_{\rm n}}$'s probes changes up to $\sim 1\,$d.

The normalized variance in the continuum expected from Poisson noise is $\sigma^2_{\rm n,exp}(\lambda) = \sigma^2_{\rm n}(\lambda)(\sqrt{\bar{I}}/\bar{I})^2$. The zero-variability level $\sqrt{\sigma^2_{\rm n,exp}}$ is shown as dashed line in the bottom panels of Fig. 2. Its comparison with the $\sqrt{\sigma^2_{\rm n}}$'s shows clear signs for variability in the line profile. Throughout the time series, the variance profile (i.e. variability as a function of wavelength) features three distinct peaks, roughly at positions of $-100... -150$, $-20... +20$, and $+100...+150\,$km/s. We note that the same structure was seen by Scholz & Jayawardhana (2006) in their Hα time series of 2M 1207. The position of these peaks (indicating the velocities of maximum changes in the Hα flux) is roughly coinciding with the position of the two maxima and the minimum in the Hα profile.

The variance profile yields only the time average of the changes as a function of wavelength. To study the profile variations in more detail we examine the change of the flux between consecutive spectra across the line. The relative flux change is given by

$$D_{\rm ji}(\lambda) = \frac{1}{2} \times \frac{I_{\rm n,j}(\lambda) - I_{\rm n,i}(\lambda)}{I_{\rm n,j}(\lambda) + I_{\rm n,i}(\lambda)}, \tag{2}$$

where $I_{\rm n}(\lambda)$ is the normalized profile, i is a running number denoting the exposures and $j = i + 1$. These relative flux changes $D(\lambda)$ are used to investigate variations as a function of the time lag between two spectra (Johns & Basri 1995). To this end, the $D(\lambda)$'s are computed not only for two subsequent spectra but for all pairs of the 59 spectra from May 8-9, 2006, i. e. for each time lag $\delta t = t2 - t1 > 0$ sampled by our UVES data. Then, we group the $D(\lambda)$'s in time lag bins of 1 h (Δt) and calculate the standard deviation $\sigma_{\Delta \rm t}(\lambda)$ of the $D(\lambda)$'s in each of these bins. Finally, we calculate for each time bin the average of these standard deviations over the whole line profile ($\bar{\sigma}_{\Delta \rm t}$). The result is shown in Fig. 5, where the numbers on top of the panel indicate the number of data points in each of the time lag bins. The gap is produced by the absence of observations with time lags between $\approx 9...16$ h, i.e. the data to the left of this gap corresponds to spectra from the same night, and the data to the right corresponds to spectra from two different nights. The level of profile variability doubles from ~ 2 % for the shortest time lag (1 h) to a maximum of ≈ 4 %, that is reached for a timelag of ~ 8 h.

To test whether the variations are correlated across the line profile we computed the correlation coefficient for each pair of spectral bins using the profiles $\bar{I}_{\rm i}(\lambda)$, with $i = 1, ..., N$. This results in a correlation matrix $r_{\rm i,j}$ of dimension $N_{\rm b} \times N_{\rm b}$, where $N_{\rm b}$ is the number of spectral bins. The confidence level of each coefficient in the matrix is computed using the error function

$$E_{\rm i,j} = \frac{\mid r_{\rm i,j} \mid \sqrt{N_{\rm b}}}{\sqrt{2}}, \tag{3}$$

such that $1 - E_{\rm i,j}$ is the confidence level for the correlation to be true.

The correlation matrix has been computed for different subgroups of Hα profiles from the UVES run. Fig. 6 displays the most interesting correlation matrices $r_{\rm i,j}$ as contour plots. Only values with confidence level > 99.9 % are considered in this representation. The first two diagrams from the left represent the matrices of each 19 consecutive spectra, obtained in the first and the second observing night, respectively. The cross-shaped pattern seen in the leftmost diagram is peculiar. The center of the cross is offset by $\approx +25$ km/s to the red side, and it represents the spectral region near the minimum of the line profile (see Fig. 1). Closer examination shows that this pattern stems from a short time interval. This is demonstrated in the rightmost diagram of Fig. 6, that displays the correlation matrix for exposures $i = 7, ..., 10$, roughly corresponding to the second average profile in the leftmost panel of Fig. 2. Clearly, during this time interval, the profile changes near the absorption minimum are uncorrelated with all velocities except for the velocities in close vicinity. The double-square shaped pattern observed during the second night (middle panel of Fig. 6) is more typical (cf. Johns & Basri 1995). The absence of contours in the upper left and in the lower right of this graph means that red and blue wings vary in an uncorrelated fashion. The range near $v \approx +75$ km/s, corresponding to the position of the right emission peak, is particularly well correlated with the whole line.

3.2. Other signatures of accretion

Our high S/N UVES spectra allow us to present the first time series for other optical emission lines of 2M 1207. In particular, we detect the Balmer lines up to Hϵ. This latter one is partly blended with Ca II H λ3968.

The shape of the Hβ profile follows closely that of Hα discussed in detail above. All higher Balmer lines are predominantly characterized by a double-peaked profile, but at times turn into a single-peaked shape. This is demonstrated in Fig. 7, that shows the contemporaneous Balmer series for two epochs. Each panel in Fig. 7 is obtained from an 8-frame average. When present, the absorption minimum is found at roughly the same position for all Balmer lines, but the ratio of the emission fluxes left and right of the minimum decreases systematically for the higher Balmer lines, i.e. the lower Balmer lines are red-dominated and the higher Balmer lines are blue-dominated.

In contrast to the Balmer lines, the Ca II H+K emission is narrow with FWHM of only ~ 20 km/s (see Table 2). Furthermore, we detect several lines of He I (λ4471, λ5876, λ6678, λ7066) and the Ca II infrared triplet (hereafter Ca IRT) in emission. All these lines are predominantly detected in accretors and, therefore, thought to be related to the accretion process. The Ca II λ8662 flux was shown to be directly related to the mass accretion rate (Mohanty et al. 2005). The three lines of the Ca IRT appear with roughly similar strength, inconsistent with formation in an outflow (Reipurth et al. 1986; Fernández & Comerón 2001). No Na D emission is seen, consistent with the prediction of magnetospheric accretion models for low accretion rates (Muzerolle et al. 2001).

We measured $W_{\rm EQ}$ and the FWHM of the stronger ones of the emission lines discussed above. The continuum was estimated from two 5 Å wide line-free regions left and right of the respective line. The observed range of $W_{\rm EQ}$ is reported for each line in Table 2 together with its approximate uncertainty. Given the often loose use of equivalent widths in the literature, it seems appropriate to stress that $W_{\rm EQ}$ is associated with considerable errors in objects with faint continuum. This is clear from the numbers given in Table 2. The errors cited in that table do not include systematic uncertainties, again affecting mainly the (faint) continuum, that we discovered in the process of defining the sky extraction area. Since we are interested in relative changes within the UVES dataset, systematic uncertainties are not a big concern. However, they should be kept in mind when comparing data obtained with different instruments, and analysed in different ways by different astronomers.

All emission lines are stronger in the second night of the UVES observations, and they are particularly weak towards the end of the first night (around MJD 53863.25 = UT 05 h on May 8, 2006). At the same moment the shape of some of the strongest emission lines underwent a change: (i) He I λ5876 temporarily becomes flat-topped and symmetrical, while it is markedly asymmetric with an extended red wing throughout most of the two nights (see Fig. 8); (ii) in Hα the 10 % width is at its minimum, and the deficiency in the red vs. the blue peak is particularly strong; (iii) in the higher Balmer lines the red portion of the line disappears almost completely, and (iv) some of the weaker lines nearly disappear at the same time.

4. Discussion

4.1. Spectral variability

We have examined the optical emission line variability of 2M 1207 at high spectral resolution in data obtained at various epochs through February, April, and May 2006. In particular, we present for the first time a near continuous spectral sequence from two consecutive nights with a time-resolution of $\approx$ 12 minutes. The study presented here complements previous work that was characterized by much poorer temporal sampling.

4.1.1. Short timescales (days to hours)

Scholz et al. (2005a) have attributed the drastic changes of the Hα line profile seen in earlier high-resolution spectra of 2M 1207 to varying viewing angle of the accretion column(s) over the course of the brown dwarf's rotation cycle. The absorption component seemed to appear and reappear on a time-scale of $\sim$ 1 day, an interval approximately coincident with the expected rotation period, therefore suggesting that the accretion spots moved with respect to the observer. However, with a maximum of 3 spectra per night, the available data did not provide adequate sampling across the presumed rotation cycle.

Within the two nights of near-continuous observation in May 2006 there is clear variability present in the Hα emission and other emission lines, albeit much less pronounced and systematic than expected from previous data. Here, we summarize its characteristics: (i) The line profile is double-peaked throughout the two nights, displaying the central absorption reversal characteristic for accretion in star-disk systems seen near edge-on; (ii) the absorption feature moves between $-10... + 40$ km/s; (iii) the absorption minimum widens twice during the observations with a time interval of ~ 23 h; (iv) variability across the line is inferred from the variance profile and the correlation matrix; and (v) the line flux varies by a factor of ≈ 6, correlated with the (small) variations of the 10 % width.

The variable redshift and width of the absorption minimum implies that the viewing angle of the absorbing layers of the accretion column changed throughout the observation. Bouvier et al. (2003) explained the radial velocities of the redshifted absorption components of the TTS AA Tau with changes in the structure of the magnetosphere. In this scenario, during times of high observed absorption redshift an observer at high inclination looks flat onto the magnetic field lines that carry the absorbing material, while low absorption redshift implies a large angle between the absorbing material and the line-of-sight. The different viewing angles can be realized by inflating or deflating the star-disk field. In the case of 2M 1207, the observed changes that occur on time-scales shorter than the rotation period may suggest that the magnetosphere is somewhat inhomogeneous across stellar longitude. However, the changes are not as dramatic as seen before. The range of observed redshifts in the absorption minimum of 2M 1207 is comparable to that of AA Tau but there is no blueshifted absorption. Therefore, for 2M 1207 outflows do not play a significant role in the formation of the Hα line.

Although there is no obvious periodicity, the rotation of the star is the most likely cause of the short-term changes of the Hα profile summarized above. We have shown that the fractional profile changes reach a maximum after a time-lag of ~ 8 h, and they remain high on a plateau for larger timelags. (The exact position of the maximum is unclear due to the absence of data with timelags between $9 - 15$ h.) This timescale is roughly consistent with one half the expected rotation period, and therefore with the time interval in which maximum changes due to rotational effects are expected.

If possible contributions from chromospheric activity and winds are neglected, the emission line flux is expected to be a measure for the accretion rate, and this is supported by its correlation with the 10 % width. This correlation is not trivial because the fit function's normalization is independent of its width, unlike in a 'canonical' Gaussian. We conclude, from the correlation observed between the equivalent widths of the emission and the absorption components (Fig. 4) that the amount of absorbing material is proportional to the total amount of material crossing the line-of-sight.

With the exception of the Ca II H + K lines, the strong emission lines (higher Balmer lines, He I and Ca IRT) follow the Hα emission closely in their shape and variability, indicating a common origin, i.e. accretion, and chromospheric contributions are not significant. In particular, throughout our observations the lines of the Balmer series are mostly double-peaked. Only the higher lines Hδ and Hϵ at times turn into a single-peaked shape.

4.1.2. Intermediate timescales (weeks to months)

The Hα line is characterized by a double-peaked profile in all spectra obtained from February to May 2006. In the spectra from February and April the redshift of the absorption feature is systematically larger with respect to the observations from May of the same year, and consequently the line profiles observed in February and April are also more asymmetric than the ones from May. However, in the data from 2006 the variations are smoother and less dramatic than the ones from 2005, for which Scholz et al. (2005a) reported alternating single- and double-peaked profiles within individual observing nights.

If the previous assumption of a high-inclination system rotating at a rate of $\sim$ 1 d is correct, the data from 2006 are compatible with a rather homogeneous distribution of accretion elements, i.e. magnetosphere, across the (sub)stellar longitudes, with smaller inhomogeneities as discussed in Sect. 4.1.1. In contrast, during 2005 the absorption reversal appeared and disappeared within one rotation cycle, implying strong variations in the accretion structure across the stellar surface. We conclude that the distribution of the accretion elements or the structure of the magnetosphere has changed within $\sim$ 1 yr. In both years, 2005 and 2006, the mass accretion rate, as inferred from the 10 % width of the Hα emission (see e.g. Natta et al. 2004, and Sect. 4.2), has shown fluctuations by a factor $\sim$ 2 on time-scales of weeks to months (cf. Table 1).

4.1.3. Long timescales (years)

Three years have passed since the first high-resolution spectrum of 2M 1207 was obtained, and in this period there seems to be a tendency towards enhanced mass accretion rate. Note, however, that the large Hα equivalent width measured by Gizis (2002) in a low-resolution spectrum counteracts this trend, and fluctuations on shorter timescales (discussed above) may be superposed on the long-term evolution. Further observations are required to confirm our speculation about the secular evolution of the Hα emission.

4.2. Accretion rate and magnetic field

Natta et al. (2004) have parametrized the accretion rate as a function of $W_{10\,\%}$ for TTS and brown dwarfs. From their Eq. 1, we find an accretion rate of $10^{-10.1...-9.8}\,M_{\odot}$/yr for the range of H$\alpha$ 10 % widths measured for 2M 1207 during the UVES run in May 2006. In previous measurements, $\dot{M}_{\rm acc}$ was as low as $\sim 10^{-11.2}\,M_{\odot}$/yr, i.e. 2M 1207 changes its accretion rate by a factor of 2 on the timescale of days, and at least by one order of magnitude over the years.

In Fig. 9 we put 2M 1207 in the context with other accreting (sub)stellar objects. A correlation between accretion rate and mass ($\dot{M}_{\rm acc} \sim M^{\alpha}$ with $\alpha \approx 2$) has been reported in the literature. In Fig. 9 we display this relation using data from the references given in Muzerolle et al. (2005). The range of $\dot{M}_{\rm acc}$ inferred from all available data of 2M 1207 is indicated by large circles connected by a vertical line.

Various explanations have been proposed for the correlation between $\dot{M}_{\rm acc}$ and M, and its large (> 2 dex) scatter. Padoan et al. (2005) see in the $\dot{M}_{\rm acc} - M$ relation a consequence of large-scale Bondi-Hoyle accretion. In their scenario, the scatter is produced by the different physical conditions in different star forming environments. Alexander & Armitage (2006) assumed that the $\dot{M}_{\rm acc} - M$ relation reflects the initial parameters of the disk-star system, and they showed that the scatter can be reproduced by a combination of varying disk initial parameters and the viscous evolution of the disk in the course of which the mass accretion rate decreases. According to Gregory et al. (2006) the $\dot{M}_{\rm acc} - M$ relation arises naturally from models of magnetospheric accretion assuming a realistic field geometry. Finally, Mohanty et al. (2005) suggested declining disk ionization with decreasing stellar mass as the origin of the $\dot{M}_{\rm acc} - M$ relation, implying that most of the scatter is due to intrinsic variability in accretion rates. This view was disputed by Natta et al. (2006) who did not find strong variations of the near-IR emission lines indicative of accretion in a sample of 14 objects from the ρ Oph star forming region. On the other hand, it has been demonstrated for a few examples of individual objects, that indeed accretion rates do vary substantially (Gullbring et al. 1996; Alencar et al. 2005; Scholz et al. 2005a; Scholz & Jayawardhana 2006). We point out that the range of mass accretion rates derived for 2M 1207 is comparable to the spread in the $\dot{M}_{\rm acc} - M$ relation. Therefore, variability might indeed explain this spread. Repeated measurements of $\dot{M}_{\rm acc}$ for known accretors will be helpful to verify our suggestion.

An alternative method to derive accretion rates has been proposed by Mohanty et al. (2005). They established that both classical TTS and brown dwarfs follow a linear correlation between the Ca II λ8662 emission flux and $\dot{M}_{\rm acc}$ determined independently from Hα modeling or veiling measurements. Following their recipe, we estimate the continuum flux $F_{\rm cont}$ of 2M 1207 at 8662 Å from the synthetic DUSTY spectra of Allard et al. (2000). We adopt

$T_{\rm eff} = 2800\,{\rm K}$, $\log g = 4.0$, and negligible veiling (see discussion in Mohanty et al. 2005, for justification of these choices). The line flux is then given by $F_{\rm CaII} = F_{\rm cont} \cdot W_{\rm EQ}$. For the highest equivalent width measured in May 2006 this results in $\log F_{\rm CaII}\,[{\rm erg/cm^2/s}] \approx 5.1$, and the fit relation for the low-mass sample of Mohanty et al. (2005) yields an accretion rate of $\dot{M}_{\rm acc} \approx 10^{-10.3}\,{\rm M_\odot/yr}$. This is in rough agreement with the value we derived above from the Hα 10 % width. We caution, that using the Ca II λ8662 line for estimating the mass accretion rate assumes a negligible contribution from activity. This seems to be true for brown dwarfs on a statistical basis ('the λ8662 component occurs almost exclusively in accreting objects'; Mohanty et al. 2005), and for 2M 1207, in particular, by the lack of measureable effects from chromospheric emission in other lines.

According to Koenigl (1991) the mass accretion rate of TTS is related to their magnetic field strength, $B \sim \dot{M}^{1/2} \cdot M_*^{1/4} \cdot R_*^{-3} \cdot R_{\rm t}^{7/4}$. We assume $R_{\rm t} \sim 2R_*$ for the disk truncation radius (Muzerolle et al. 2000). The mass and radius of 2M 1207 are $M_* = 0.03\,M_\odot$ and $R_* = 0.27 R_\odot$ (Chabrier et al. 2000). Taking account of the scaling factors, the average accretion rate of 2M 1207 observed in May 2006 ($\dot{M} \sim 10^{-10}\,{\rm M_\odot/yr}$) yields an approximate value for the surface field, $B \approx 200\,{\rm G}$. The same equation yields for a TTS with $0.8\,{\rm M_\odot}$, $1.5\,{\rm R_\odot}$, and $\dot{M} \sim 10^{-8}\,{\rm M_\odot/yr}$ a surface field of $\approx 600\,{\rm G}$. This validates the remark made by Scholz & Jayawardhana (2006) who, without citing numbers for the field strength, had argued that the magnetic field for a typical brown dwarf is expected to be roughly half that of a typical TTS. The magnetic field of TTS obtained this way is somewhat lower than measured values, which are typically in the kilogauss range (e.g. Yang et al. 2005, and references herein). There are, however, considerable uncertainties connected with the use of the Koenigl-relation, such as the simplified assumption of a dipolar field and the location of the inner disk radius with respect to the corotation radius that determines the scaling factor. Given these ambiguities, the order of magnitude agreement between the estimated and observed fields is plausible.

4.3. Accretion versus activity in TWA brown dwarfs

Given the presence of a magnetic field, inferred from the accretion rate, the absence of strong magnetic activity on 2M 1207 is remarkable. A very stringent upper limit to its X-ray emission was placed by a 50 ksec *Chandra* observation (Gizis & Bharat 2004). The radio emission was constrained to the lowest value among the brown dwarfs in the TWA (Osten & Jayawardhana 2006). In Table 3 we summarize the accretion and activity measures for all four TWA brown dwarfs.

The data in Table 3 has been collected from the literature except for the X-ray data for

SSSPM 1102. This object was identified as a probable substellar TWA member in a recent proper motion study of the Supercosmos Sky Survey data (Scholz et al. 2005b). SSSPM 1102 is in the field-of-view of an archived *XMM-Newton* observation (Obs-ID 0112880201). We ran the standard Science Analysis System source detection process, and find no X-ray source at the optical position of SSSPM 1102. To estimate an upper limit to its X-ray luminosity, we measured the counts at the expected position of SSSPM 1102 and in an annulus around this position (representing the background). After applying the appropriate area scaling factor and extracting the on-source time from the exposure map, an upper limit to the net source count rate was estimated using the algorithm of Kraft et al. (1991). The distance to SSSPM 1102 has been given by Mamajek (2005) ($d \sim 43$ pc). This yields $L_{\rm x} < 5.3 \cdot 10^{26}$ erg/s in the $0.5 - 10$ keV band.

It is constructive to compare 2M 1207 to TWA-5 B, the best-studied substellar object in the TWA after 2M 1207. Matching their properties shows the dichotomy of one brown dwarf that accretes but is not magnetically active, and another brown dwarf that is magnetically active but does not accrete. Presumably, some mechanism suppresses activity in accreting substellar objects, as seems to be the case for classical TTS (Preibisch et al. 2005; Telleschi et al. 2006). Possible explanations that have been put forth in the context of classical TTS are changes in the magnetic field structure and/or heating process of the corona as a result of accretion. The absence of magnetic activity on 2M 1207 is further surprising, as accreting substellar objects with similar magnetic field strength, e.g. V410 Anon 13, have been shown to be X-ray emitters (Muzerolle et al. 2000; Güdel et al. 2006). For the substellar regime, the relation between accretion and X-ray luminosity has not yet been established on a statistical sample. If such a relation, as suggested by 2M 1207 and TWA-5 B, is confirmed, this would provide one more piece of evidence for the TTS-like character of brown dwarfs. X-ray and radio studies of the remaining two TWA brown dwarfs, both of which are non-accreting, should be useful.

5. Conclusions

A substantial number of high-resolution spectroscopic observations has been collected for the brown dwarf 2M 1207. These data have allowed us to study its accretion variability on timescales from hours to ~ 3 yrs. While small variations are obviously present throughout the rotation (~ 1 d), major changes in the structure of accretion may take place over months or years. A summary of all Hα width measurements suggests a trend towards increasing accretion rate during the last three years. However, it is not clear if this trend reflects erratic changes or a systematic evolution. All in all, our dedicated monitoring has shown that the accretion pattern on 2M 1207 is probably more complex than expected. It comprises, longterm changes of the accretion rate and (maybe independently) of the flow structure (months to years), variations on the timescale of the rotation rate (hours to days), and possibly on even shorter timescales as suggested by our high temporal resolution data.

2M 1107 is among the lowest mass dwarfs with measured mass accretion rate. The values derived from the various observations obtained in a time-span of $\sim 3\,$yrs, differ by nearly 2 dex, similar to (and possibly explaining) the scatter observed in the relation between accretion rate and stellar mass. Whether accretion variability is decisive for shaping the $\dot{M}_{\rm acc} - M$ relation will be established in future systematic spectroscopic studies across a wide mass range.

This paper is based on data collected under the ESO program 077.C-0323. BS acknowledges financial support from ASI contract ASI-INAF I/023/05/0. BS wishes to thank S. Randich and S. Mohanty for useful discussions on the UVES pipeline analysis and brown dwarf emission line spectra. RJ and AS acknowledge support from an NSERC grant to RJ.

Facility: VLT:Kueyen (UVES)

REFERENCES

Alencar, S. H. P., Basri, G., Hartmann, L., & Calvet, N. 2005, A&A, 440, 595

Alexander, R. D., & Armitage, P. J. 2006, ApJ, 639, L83

Allard, F., Hauschildt, P. H., & Schweitzer, A. 2000, ApJ, 539, 366

Allers, K. N., Kessler-Silacci, J. E., Cieza, L. A., & Jaffe, D. T. 2006, ApJ, 644, 364

Ballester, R., Modigliani, A., Boitquin, O., Cristiani, S., Hanuschik, R., Kaufer, A., & Wolf, S. 2000, in The Messenger, Vol. 101, 31

Barrado y Navascués, D., Mohanty, S., & Jayawardhana, R. 2004, ApJ, 604, 284

Bouvier, J., Grankin, K. N., Alencar, S. H. P., Dougados, C., Fernández, M., Basri, G., Batalha, C., Guenther, E., Ibrahimov, M. A., Magakian, T. Y., Melnikov, S. Y., Petrov, P. P., Rud, M. V., & Zapatero Osorio, M. R. 2003, A&A, 409, 169

Burgasser, A. J., & Putman, M. E. 2005, ApJ, 626, 486

Chabrier, G., Baraffe, I., Allard, F., & Hauschildt, P. 2000, ApJ, 542, 464

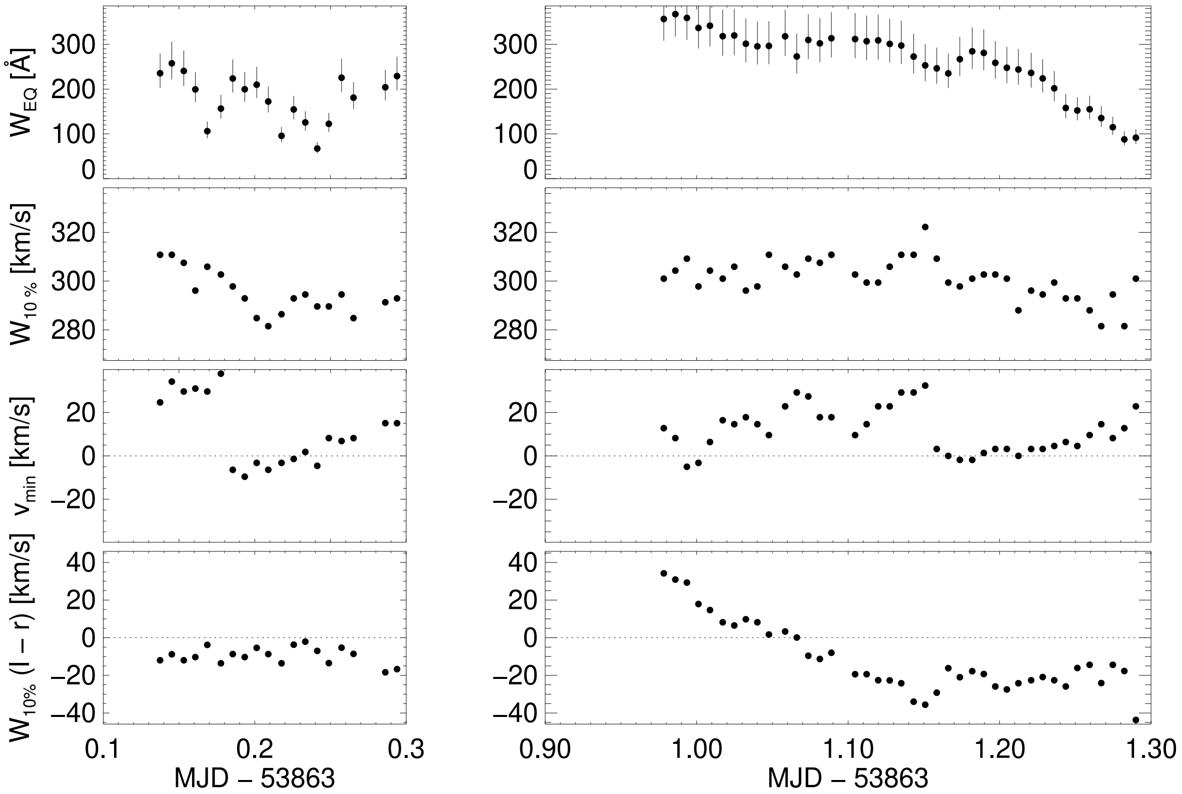

Fig. 1.— Temporal evolution of parameters characterizing the Hα emission of 2M 1207 during May 8-9, 2006.

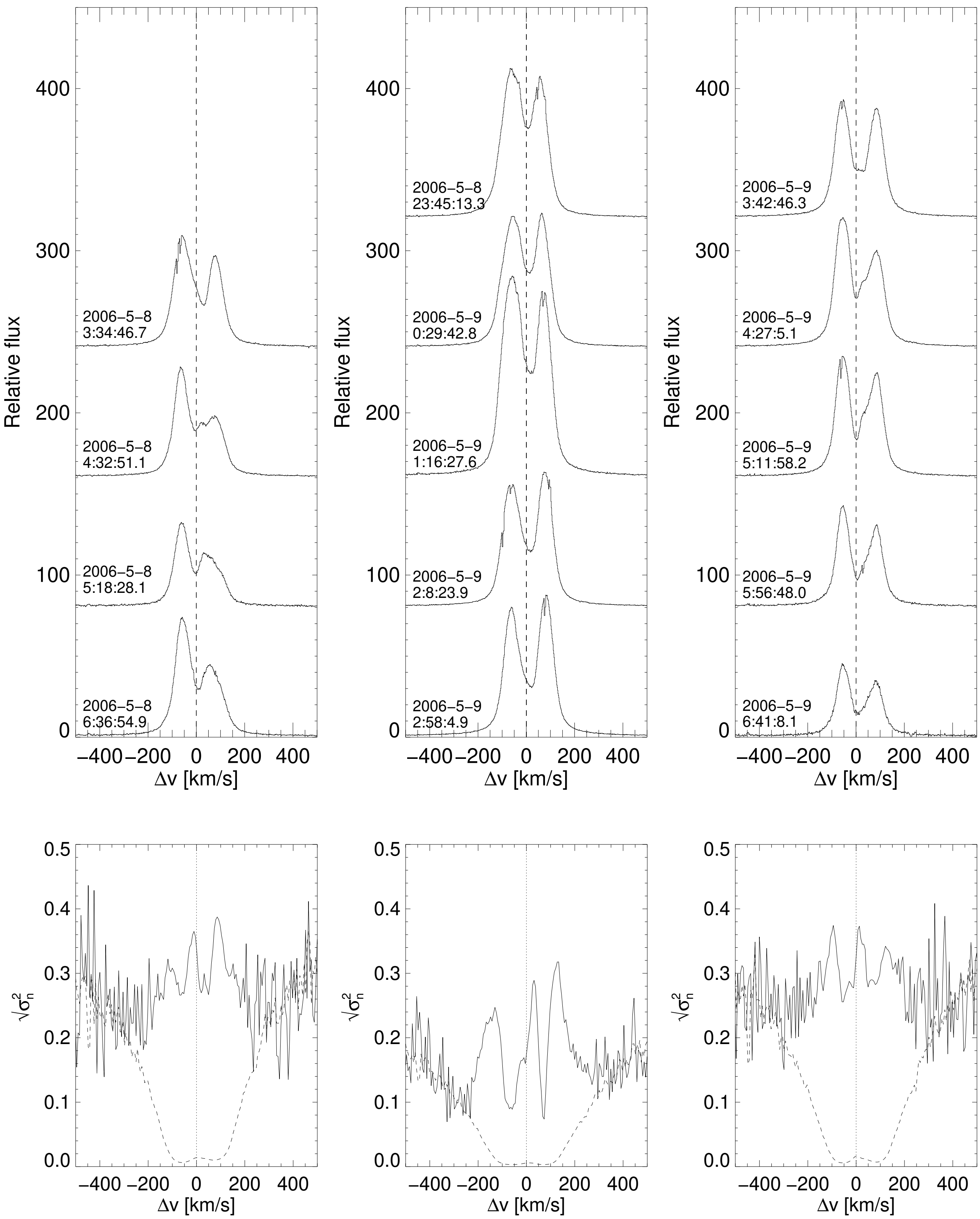

Fig. 2.— *top* – Normalized average Hα line profiles of 2M 1207 obtained with UVES in May 2006; *bottom* - Normalized variance line profiles and zero-variability level.

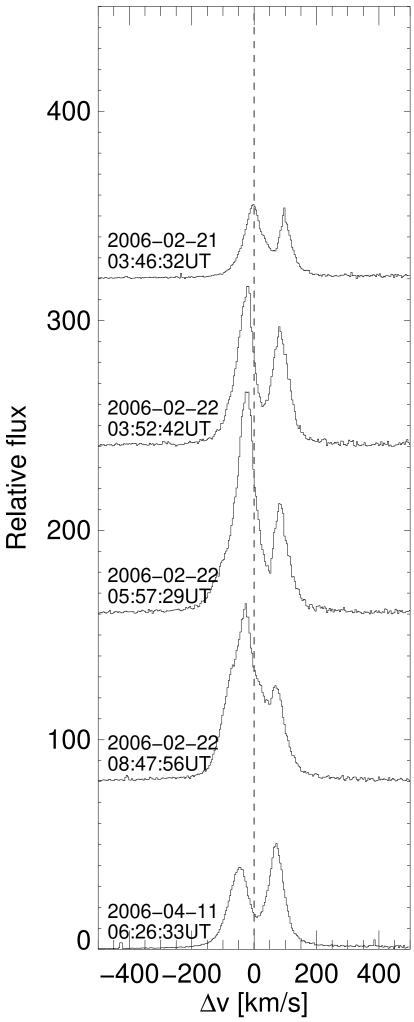

Fig. 3.— Hα line profiles of 2M 1207 obtained with MIKE in Feb and Apr 2006. The data were normalized to the average continuum level near the line.

Table 1: Summary of Hα width measurements for 2M 1207.

Date	$W_{10\,\%}$ [km/s]	Reference
Apr 2002	$\sim 300^{\dagger}$	Gizis (2002)
May 8, 2003	170...200	Mohanty et al. (2003)
Jan 29 - Feb 1, 2005	209...215	Scholz et al. (2005a)
Mar 17 - 19, 2005	253...308	Scholz et al. (2005a)
Mar 27 - 30, 2005	279...304	Scholz et al. (2005a)
Feb 21 - 22, 2006	261...281	present work
Apr 11, 2006	253	present work
May 8 - 9, 2006	281...322	present work
May 16, 2006	320	Whelan et al. (2007)

† low-resolution data, no 10 % width measured.

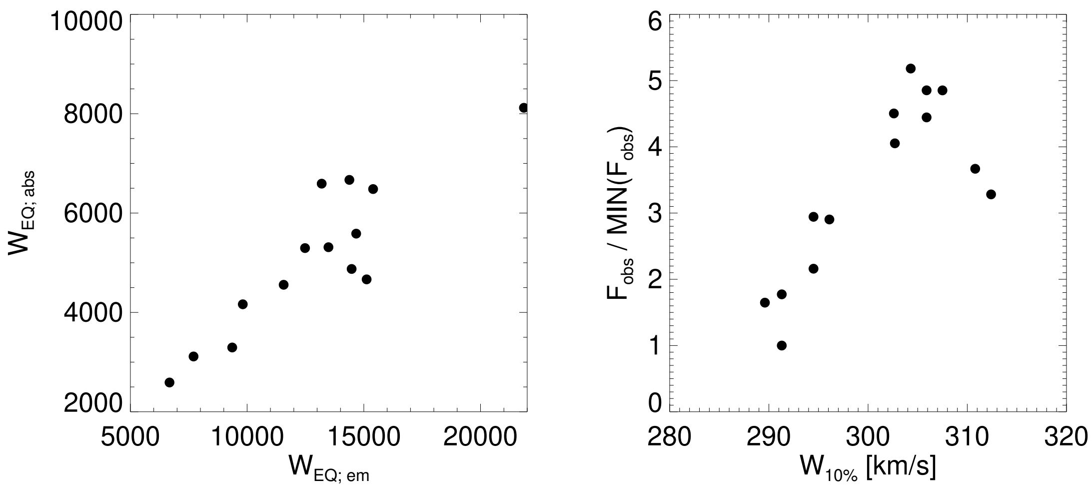

Fig. 4.— Equivalent widths of Gaussian fits to the emission ($W_{\mathrm{EQ;em}}$) and absorption ($W_{\mathrm{EQ;abs}}$) component of the Hα line, and normalized total observed flux ($F_{\mathrm{obs}} = F_{\mathrm{em}} - F_{\mathrm{abs}}$) versus H$\alpha$ 10 % width.

Table 2: Equivalent widths and FWHM for detected emission lines.

Identification	$W_{\rm EQ}^{(a)}$ [Å]	typ.error$^{(a,b)}$ [Å]	FWHM$^{(c)}$ [km/s]
Hβ	4.5...47.1	~ 6	180
Hγ	0.3...13.5	~ 2	180
Hδ	...	...	168
Hϵ+Ca II H	...	...	144
Ca II K	...	...	18
He I λ5876	1.8...9.1	~ 2	30
Hα	145...394	~ 45	210
He I λ6678	0.9...2.4	~ 2	18
Ca II λ8498	0...0.6	~ 0.35	12
Ca II λ8542	0...0.3	~ 0.25	12
Ca II λ8662	0...0.4	~ 0.3	12

$^{(a)}$ No equivalent widths are given for the higher Balmer lines and for Ca II H+K because of the low continuum
$^{(b)}$ Errors for the equivalent width are estimated by assuming a 15 % uncertainty in the continuum flux.
$^{(c)}$ measured in an average spectrum that represents the typical line profile for 2M 1207 during the observation.

Table 3: Activity and accretion measures of all known brown dwarfs in TWA.

Designation	IR excess	$W_{{\rm H}\alpha;10\,\%}$ [km/s]	$L_{\rm x}$ [erg/s]	$L_{\rm R}$ [10^{14} erg/s/Hz]	FUV	Refs
TWA 5B		162	$4\,10^{27}$	< 2.0		(-,1,2,3,-)
2M 1207	$\surd$	170...320	$< 1.2\,10^{26}$	< 0.98	$\surd$	(4,5,6,3,7)
2M 1139	–	111	?	?		(4,1,-,8,-)
SSSPM 1102		194	$< 5.3\,10^{26}$	< 1.6		(-,1,9,3,-)

(1) - Mohanty et al. (2003), (2) - Tsuboi et al. (2003), (3) - Osten & Jayawardhana (2006), (4) - Riaz et al. (2006), (5) - see references in this paper, (6) - Gizis & Bharat (2004), (7) - Gizis et al. (2005), (8) - Burgasser & Putman (2005), (9) - this paper.

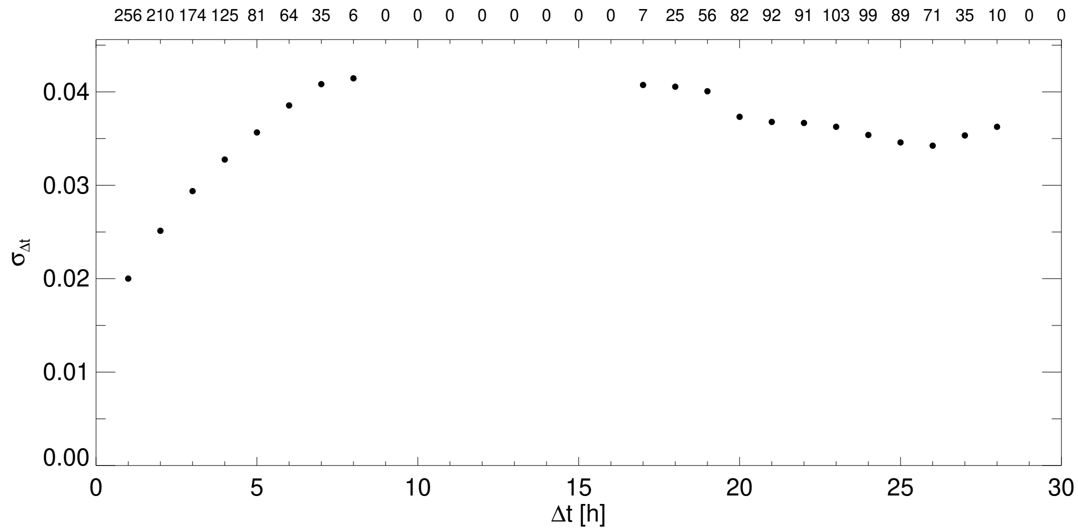

Fig. 5.— Mean of the standard deviation of fractional profile changes $D(\lambda)$ in the Hα line as a function of time lag. Numbers on top of the panel indicate the number of data points in each of the time lag bins.

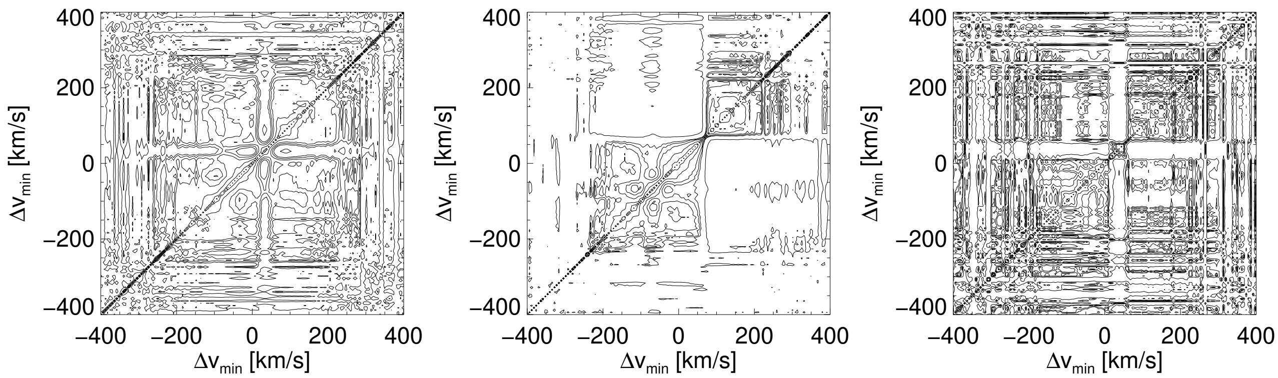

Fig. 6.— Correlation matrix of Hα for different subset of exposures (denoted i) obtained on May 8-9, 2006. *left* – $i = 1, ..., 19$; *middle* – $i = 20, ...38$; *right* – $i = 7, ..., 10$.

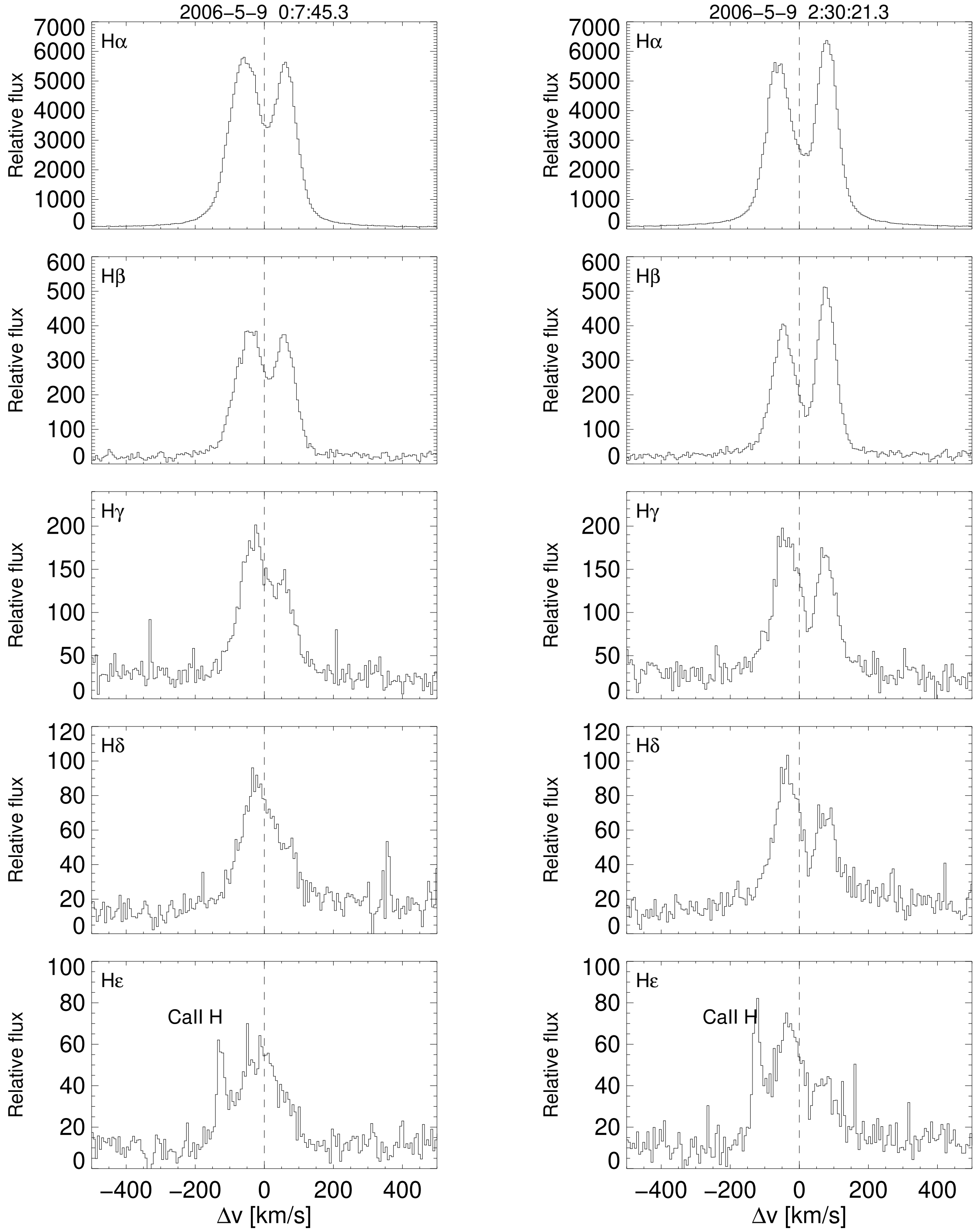

Fig. 7.— Contemporaneous Balmer emission line profiles (Hα to Hϵ) for two epochs during the UVES run (8-frame averages).

Chauvin, G., Lagrange, A.-M., Dumas, C., Zuckerman, B., Mouillet, D., Song, I., Beuzit, J.-L., & Lowrance, P. 2004, A&A, 425, L29

—. 2005, A&A, 438, L25

Edwards, S., Cabrit, S., Strom, S. E., Heyer, I., Strom, K. M., & Anderson, E. 1987, ApJ, 321, 473

Fernández, M., & Comerón, F. 2001, A&A, 380, 264

Gizis, J. E. 2002, ApJ, 575, 484

Gizis, J. E., & Bharat, R. 2004, ApJ, 608, L113

Gizis, J. E., Shipman, H. L., & Harvin, J. A. 2005, ApJ, 630, L89

Gregory, S. G., Jardine, M., Simpson, I., & Donati, J.-F. 2006, MNRAS, 371, 999

Güdel, M., Briggs, K. R., Arzner, K., Audard, M., Bouvier, J., Feigelson, E. D., Franciosini, E., Glauser, A., Grosso, N., Micela, G., Monin, J. ., Montmerle, T., Padgett, D. L., Palla, F., Pillitteri, I., Rebull, L., Scelsi, L., Silva, B., Skinner, S. L., Stelzer, B., & Telleschi, A. 2006, ArXiv Astrophysics e-prints

Gullbring, E., Petrov, P. P., Ilyin, I., Tuominen, I., Gahm, G. F., & Loden, K. 1996, A&A, 314, 835

Hamann, F. 1994, ApJS, 93, 485

Hartigan, P., Edwards, S., & Ghandour, L. 1995, ApJ, 452, 736

Hartmann, L., Hewett, R., & Calvet, N. 1994, ApJ, 426, 669

Jayawardhana, R., Ardila, D. R., Stelzer, B., & Haisch, Jr., K. E. 2003a, AJ, 126, 1515

Jayawardhana, R., Mohanty, S., & Basri, G. 2003b, ApJ, 592, 282

Johns, C. M., & Basri, G. 1995, AJ, 109, 2800

Koenigl, A. 1991, ApJ, 370, L39

Kraft, R. P., Burrows, D. N., & Nousek, J. A. 1991, ApJ, 374, 344

Luhman, K. L., Lada, C. J., Hartmann, L., Muench, A. A., Megeath, S. T., Allen, L. E., Myers, P. C., Muzerolle, J., Young, E., & Fazio, G. G. 2005, ApJ, 631, L69

Mamajek, E. E. 2005, ApJ, 634, 1385

Martín, E. L. 1998, AJ, 115, 351

Mohanty, S., Jayawardhana, R., & Barrado y Navascués, D. 2003, ApJ, 593, L109

Mohanty, S., Jayawardhana, R., & Basri, G. 2005, ApJ, 626, 498

Mundt, R. 1984, ApJ, 280, 749

Muzerolle, J., Briceño, C., Calvet, N., Hartmann, L., Hillenbrand, L., & Gullbring, E. 2000, ApJ, 545, L141

Muzerolle, J., Calvet, N., & Hartmann, L. 2001, ApJ, 550, 944

Muzerolle, J., Luhman, K. L., Briceño, C., Hartmann, L., & Calvet, N. 2005, ApJ, 625, 906

Natta, A., Testi, L., Comerón, F., Oliva, E., D'Antona, F., Baffa, C., Comoretto, G., & Gennari, S. 2002, A&A, 393, 597

Natta, A., Testi, L., Muzerolle, J., Randich, S., Comerón, F., & Persi, P. 2004, A&A, 424, 603

Natta, A., Testi, L., & Randich, S. 2006, A&A, 452, 245

Osten, R. A., & Jayawardhana, R. 2006, ApJ, 644, L67

Padoan, P., Kritsuk, A., Norman, M. L., & Nordlund, Å. 2005, ApJ, 622, L61

Preibisch, T., Kim, Y.-C., Favata, F., Feigelson, E. D., Flaccomio, E., Getman, K., Micela, G., Sciortino, S., Stassun, K., Stelzer, B., & Zinnecker, H. 2005, ApJS, 160, 401

Reipurth, B., Bally, J., Graham, J. A., Lane, A. P., & Zealey, W. J. 1986, A&A, 164, 51

Riaz, B., Mullan, D. J., & Gizis, J. E. 2006, ApJ, 650, 1133

Scholz, A., & Jayawardhana, R. 2006, ApJ, 638, 1056

Scholz, A., Jayawardhana, R., & Brandeker, A. 2005a, ApJ, 629, L41

Scholz, R.-D., McCaughrean, M. J., Zinnecker, H., & Lodieu, N. 2005b, A&A, 430, L49

Sterzik, M. F., Pascucci, I., Apai, D., van der Bliek, N., & Dullemond, C. P. 2004, A&A, 427, 245

Telleschi, A., Güdel, M., Briggs, K. R., Audard, M., & Palla, F. 2006, ArXiv Astrophysics e-prints

Tsuboi, Y., Maeda, Y., Feigelson, E. D., Garmire, G. P., Chartas, G., Mori, K., & Pravdo, S. H. 2003, ApJ, 587, L51

Whelan, E. T., Ray, T. P., Randich, S., Bacciotti, F., Jayawardhana, R., Testi, L., Natta, A., & Mohanty, S. 2007, ApJ, 659, L45

White, R. J., & Basri, G. 2003, ApJ, 582, 1109

Yang, H., Johns-Krull, C. M., & Valenti, J. A. 2005, ApJ, 635, 466

This preprint was prepared with the AAS LATEX macros v5.0.

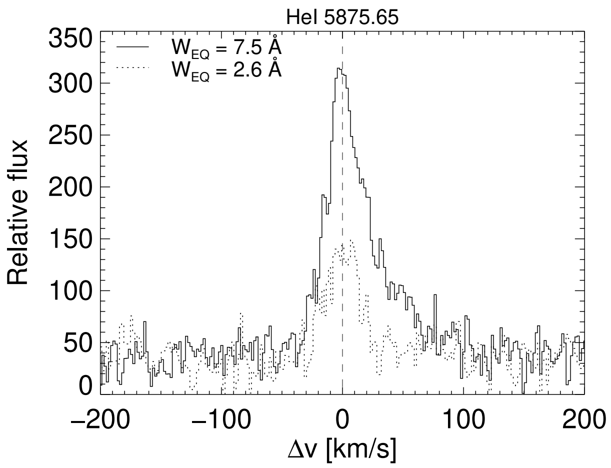

Fig. 8.— Two spectra in the region of He I λ5876 showing the change from the typical profile with extended red wing (solid line) to the weak, symmetric line (dotted line).

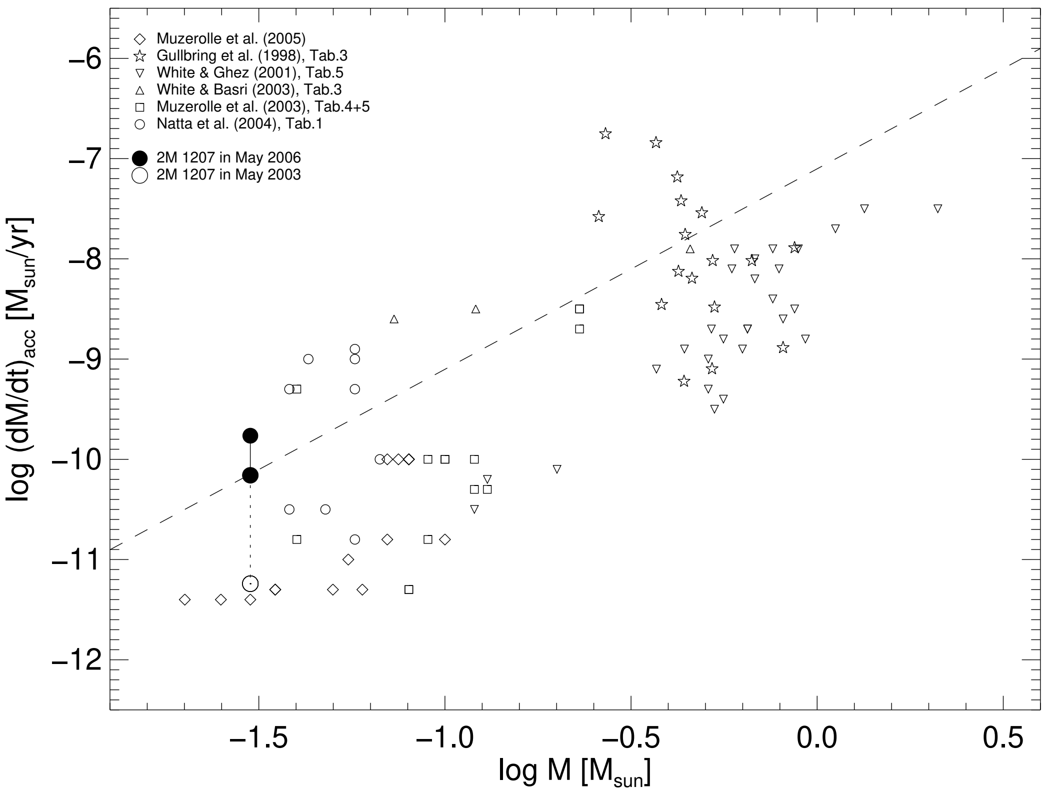

Fig. 9.— Relation between mass and mass accretion rate for sub-stellar objects; data from the literature cited by Muzerolle et al. (2005)